

Article

Effect of Pre-Strain on Microstructure and Tensile Properties of Ti-6Al-4V at Elevated Temperature

Taowen Wu , Ning Wang *, Minghe Chen, Dunwen Zuo, Lansheng Xie and Wenxiang Shi

Nanjing University of Aeronautics and Astronautics, Nanjing 210016, China; meewtw0116@nuaa.edu.cn (T.W.); meemhchen@nuaa.edu.cn (M.C.); imit505@nuaa.edu.cn (D.Z.); meelsxie@nuaa.edu.cn (L.X.); swx1996@nuaa.edu.cn (W.S.)

* Correspondence: meewn1987@nuaa.edu.cn

Abstract: Research on pre-deformation influences on material properties in multistep hot forming is of important scientific interest. In this paper, hot tensile tests at 850 °C and a strain rate of 0.001 s⁻¹ were performed to study the microstructural evolution and mechanical properties of Ti-6Al-4V with pre-strains at 0.05, 0.1 and 0.15. The tensile test results showed that the specimen with 0.05 pre-strain exhibited higher flow stress and larger elongation. Additionally, increasing the pre-strain resulted in a decrease in ultimate tensile strength (UTS) and elongation (EL). The EBSD results showed that the main deformation mechanism of Ti-6Al-4V was high-angle grain boundary sliding. Pre-strain promoted dynamic recrystallization (DRX) by increasing the deformation substructure. The refinement of grains and the eradication of dislocations enhanced the deformability, resulting in an increase in flow stress.

Keywords: Ti-6Al-4V titanium alloy; pre-deformation; dynamic recrystallization; microstructure evolution; mechanical properties



Citation: Wu, T.; Wang, N.; Chen, M.; Zuo, D.; Xie, L.; Shi, W. Effect of Pre-Strain on Microstructure and Tensile Properties of Ti-6Al-4V at Elevated Temperature. *Metals* **2021**, *11*, 1321. <https://doi.org/10.3390/met11081321>

Academic Editors: Maciej Motyka and Marcello Cabibbo

Received: 25 June 2021

Accepted: 18 August 2021

Published: 20 August 2021

Publisher's Note: MDPI stays neutral with regard to jurisdictional claims in published maps and institutional affiliations.



Copyright: © 2021 by the authors. Licensee MDPI, Basel, Switzerland. This article is an open access article distributed under the terms and conditions of the Creative Commons Attribution (CC BY) license (<https://creativecommons.org/licenses/by/4.0/>).

1. Introduction

Titanium alloys have a wide range of applications in aerospace and other industries due their high specific strength, corrosion resistance, high temperature resistance, etc. [1,2]. Ti-6Al-4V was the first titanium alloy put into structural production of which the long-term service temperature can reach 400 °C. In the aviation industry, Ti-6Al-4V is mainly used to manufacture aero-engine compressor discs and blades [3]. The alloy is composed of the hcp α phase, which plays an important role in hindering plastic deformation, and the bcc β phase [4]. However, Ti-6Al-4V has poor forming performance and strong work hardening at room temperature. Hot-forming techniques are widely used to form complicated shape parts because the formability of Ti-6Al-4V is largely improved at elevated temperature. Ti-6Al-4V has been selected to manufacture hollow aero-engine blades for weight reduction. The hollow blade forming process consists of diffusion bonding, hot twisting, hot stamping, and gas bulging. To investigate the hot twisting procedure influence on Ti-6Al-4V deformation behavior in the subsequent hot stamping process, it is necessary to study the microstructural evolution and deformation mechanisms of Ti-6Al-4V with pre-strain [5–7].

Research has been performed to reveal the relationship between the rheological properties and microstructure of titanium alloys in high-temperature deformation [8–11]. Cui et al. [8] presented a constitutive model of TC11 based on the Arrhenius-type hyperbolic sine method by the cubic piecewise function of strain which ensured the high precision of the model. Liu et al. [9] considered that the deformation and softening mechanism of the Ti55 titanium alloy under temperatures ranging from 885 °C to 935 °C were grain boundary sliding and discontinuous dynamic recrystallization, respectively. Davis et al. [10] analyzed how the process parameters affect the β -phase recrystallization level and the final grain size by controlling the specimen deformation and heating rate. In addition, some researchers have achieved excellent microstructure and mechanical properties through

multiple deformations [11,12] and proposed effective step-by-step forming methods to refine the grains of titanium alloys and increase the strength of titanium alloys [13–15].

Pre-deformation effects on microstructural and mechanical properties have also been studied. Wang et al. [16] found that pre-deformation can promote the precipitation of a stripe wall-like phase, which improves the material strength and elongation. Sachtleber et al. [17] established a relationship between pre-deformation and the grain size of 6022-T4 aluminum alloys through uniaxial tensile tests. However, little research has been conducted on the effects of pre-deformation on the microstructure and properties of titanium alloys during the hot-forming process.

The aim of this research was to study the microstructural evolution and mechanical properties of Ti-6Al-4V titanium alloys with different pre-strains during hot tensile deformation. Ti-6Al-4V specimens were first stretched by hot tensile tests at a temperature of 850 °C and strain rate of 0.001 s⁻¹ to obtain various pre-strains and microstructures. The grain size, dislocation density and dynamic recrystallization ratio were quantitatively analyzed by the electron backscatter diffraction (EBSD) technique. The deformation mechanism of Ti-6Al-4V alloy was analyzed to explain the tensile behaviors. The influence of pre-strain on the properties of the Ti-6Al-4V titanium alloy was analyzed, combined with dislocation density and dynamic recrystallization ratio, which provided a theoretical basis for the stepwise hot torsion process.

2. Materials and Methods

The chemical composition of Ti-6Al-4V titanium alloy used in this study was Ti-5.92Al-3.92V-0.108O-0.1Fe-0.02N. Before the experiment, we used Wire Electrical Discharge Machining (WEDM) to cut it into tensile specimens as shown in Figure 1a. The gauge length of the specimen was ground to reduce burrs and scratches on the surface of specimens by sandpaper. A boron nitride solder stopper was sprayed on the surface of specimens to prevent the specimen from oxidizing. Schematic diagram of hot tensile test heating path is shown in Figure 2.

All the hot tensile tests were carried out on a UTM 5504X electronic universal testing machine (SUNSTEST Inc., Shenzhen, China) equipped with an environment chamber. The experimental scheme is given in Table 1.

Table 1. Experimental schemes of hot tensile test.

Test No.	Pre-Strain	Tensile Test Parameter	Final Strains
Test-0	0	850 °C, 0.001 s ⁻¹	0.3
			0.5
			0.7
			fracture
Test-1	0.05	850 °C, 0.001 s ⁻¹	0.3
			0.5
			0.7
			fracture
Test-2	0.1	850 °C, 0.001 s ⁻¹	0.3
			0.5
			0.7
			fracture
Test-3	0.15	850 °C, 0.001 s ⁻¹	0.3
			0.5
			0.7
			fracture

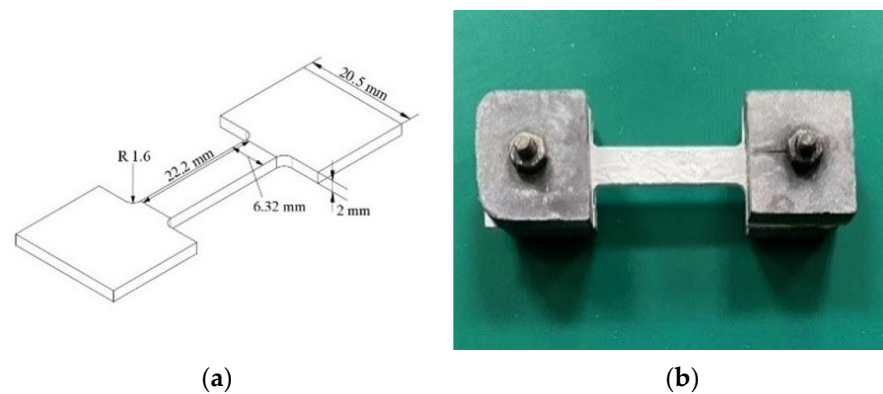


Figure 1. (a) Design of the hot tensile test specimen; (b) hot tensile fixtures.

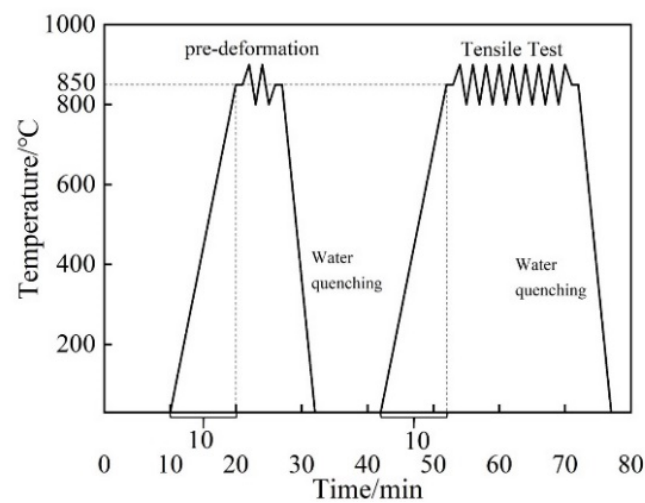


Figure 2. Schematic diagram of the Ti-6Al-4V hot tensile test heating path.

The specimens were first installed in the grips and soaked at 850 °C for 10 min. Then, they were stretched to the true strains of 0, 0.05, 0.1, and 0.15 at the strain rate of 0.001 s⁻¹, held for 10 min, and cooled in water, which represented the hot twisting process. Tensile specimens with pre-deformation were placed in the grips and soaked at 850 °C for 10 min. Then, they were stretched to the true strains of 0.3, 0.5, and 0.7 and fractured. Specimens were immediately quenched in water to retain the microstructures. For each condition, the test was repeated three times. Metallographic observations were carried out through EBSD testing. EBSD data were obtained by SIGMA 500 (ZEISS Inc., Oberkochen, Germany) and analyzed through HKL-Channel 5 software (Version 5, Oxford Instruments Inc., London, UK). XRD data were obtained by Bruker D8 advance (Bruker Inc., Karlsruhe, Germany) and analyzed through Jade (Version 6.5, Materials Data, Livemore, CA, USA).

3. Results and Discussion

3.1. Hot Tensile Properties of Specimens with Pre-Strain

Figure 3a shows the true stress-strain curve of specimens under uniaxial tension at 850 °C and 0.001 s⁻¹ with different pre-deformation strains. It is obvious that the tensile behavior was affected by the pre-deformation. Tensile properties such as yield strength (YS), ultimate tensile strength (UTS), flow stress σ ($\epsilon = 0.5$) and elongation (EL) are given in Figure 3b. It was found that the EL was more than 200%, regardless of the pre-strain, indicating that the material had superplasticity under this tensile condition [18,19]. The results show that the specimen with a pre-strain of 0.05 had the highest ultimate tensile strength and maximum elongation, which are 77.3 MPa and 234.5%, respectively. As the pre-deformation strain increased from 0.05 to 0.1, the YS decreased gradually from

63.4 MPa to 55.5 MPa, the *UTS* decreased from 77.3 MPa to 66.8 MPa, and the *EL* decreased from 234.5% to 205.2%. When the pre-strain was raised from 0.1 to 0.15, the *UTS* further declined to 61.4 MPa and the change in the *EL* was small. Additionally, Figure 3c shows the samples stretched to fracture.

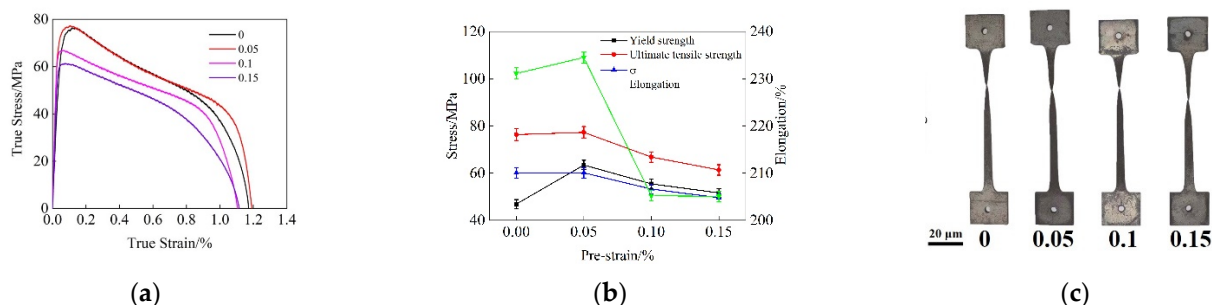


Figure 3. Hot tensile behavior of different Ti-6Al-4V specimens stretched at 850 °C with 0.001 s⁻¹: (a) True stress-strain curves; (b) Tensile properties; (c) Tested samples with different pre-strain.

3.2. Microstructure Evolution during Hot Tensile Test

Microstructures of the tensile specimens with true strains of 0.3, 0.5 and 0.7 were compared to investigate the microstructure evolution and DRX during hot deformation, which could explain the changes in the tensile properties.

3.2.1. Initial Microstructure

The microstructure and the inverse pole figure (IPF) are given in Figure 4a,b, respectively, in which the color code represents the orientations of α grains: black lines represent the high-angle grain boundaries (HAGBs, $\theta > 15^\circ$), and blue lines represent the low angle grain boundaries (LAGBs, $2^\circ < \theta < 15^\circ$). The initial structure consisted of an equiaxed α phase and intergranular β phase. Figure 4c shows the average grain size distribution, which indicates that the initial structure was mostly composed of equiaxed grains with size $\leq 2 \mu\text{m}$. The average grain size was 2.77 μm . Figure 4d shows the misorientation distribution. The fraction of LAGBs was 32.6%, and LAGBs were concentrated within 5° . HAGBs were concentrated between 55° and 65° . The abundant HAGBs indicate that the as-received material had a few deformation substructures. As shown in Figure 4e, the initial samples were composed of α and β phases.

3.2.2. Microstructures of Specimens without Pre-Strain

Figure 5 shows the microstructures and corresponding IPFs of the tensile specimens without pre-strain at different deformation stages. The average sizes of grains in specimens with different strains were 2.57 μm , 2.55 μm and 2.44 μm , respectively. The phase volume fraction changed slightly with the increasing strain because the stretching temperature was much lower than the phase transition point, which was 998 °C. The grain size decreased continuously with the increase in strain, whereas the DRX fraction increased significantly. It can be deduced that with the increase in strain, LAGBs transformed into HAGBs, and finally formed small crystal grains [20]. In the early tensile stage, the dislocation density increased rapidly with strain. Additionally, the dislocations accumulated to form LAGBs. Many small equiaxed grains appeared on the grain boundaries when the strain reached 0.5, marked by the white tip in Figure 5b. This may have been the result of dynamic recrystallization (DRX) as the subgrains with LAGBs evolved into grains with HAGBs. The abundant internal LAGBs promoted the occurrence of DRX. The merge of the subgrains and the formation of HAGBs during the hot tensile procedure caused the decrease in dislocation density, which resulted in a decrease in the flow stress. DRX plays a softening role in the deformation process. DRX is mainly divided into continuous dynamic recrystallization (CDRX), discontinuous dynamic recrystallization (DDRX), and geometric dynamic

recrystallization (GDRX), and is distinguished by the mechanism of recrystallization grain formation [21,22].

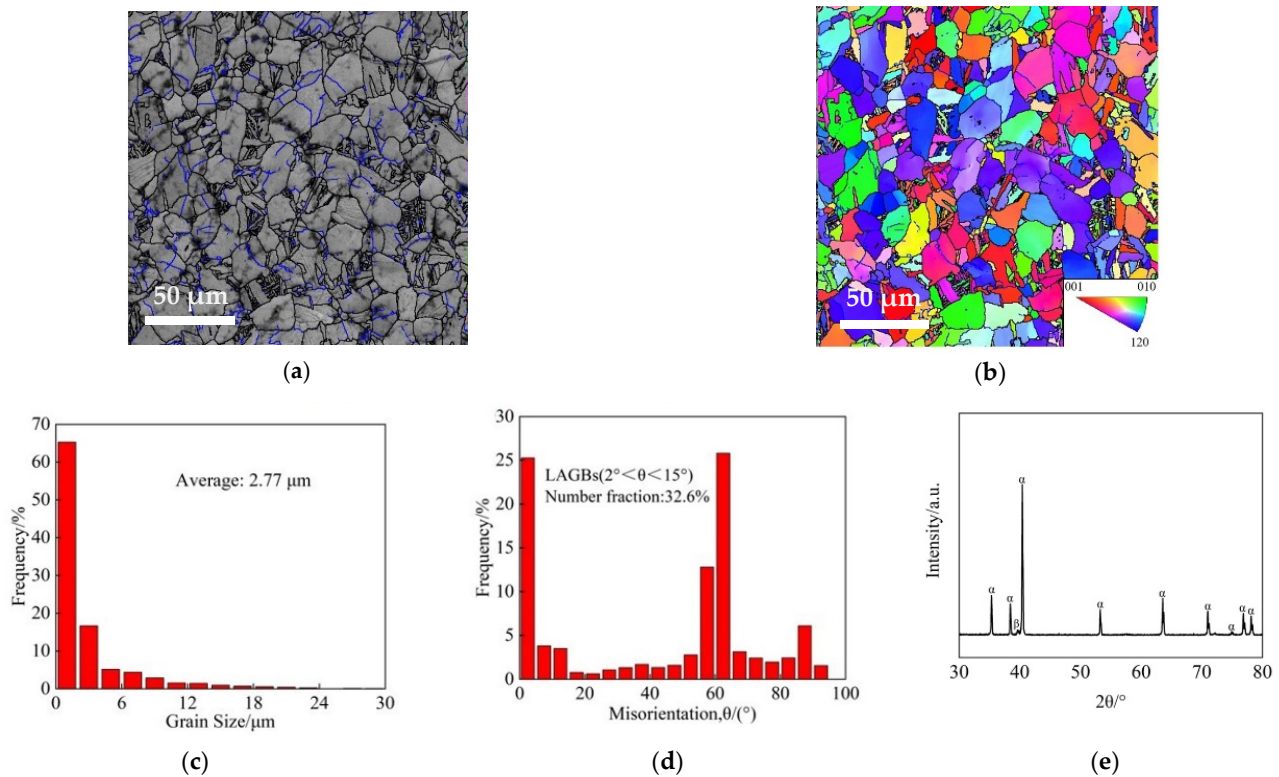


Figure 4. Characterization of initial Ti-6Al-4V: (a) SEM; (b) IPF; (c) Grain size distribution; (d) Misorientation distribution; and (e) XRD.

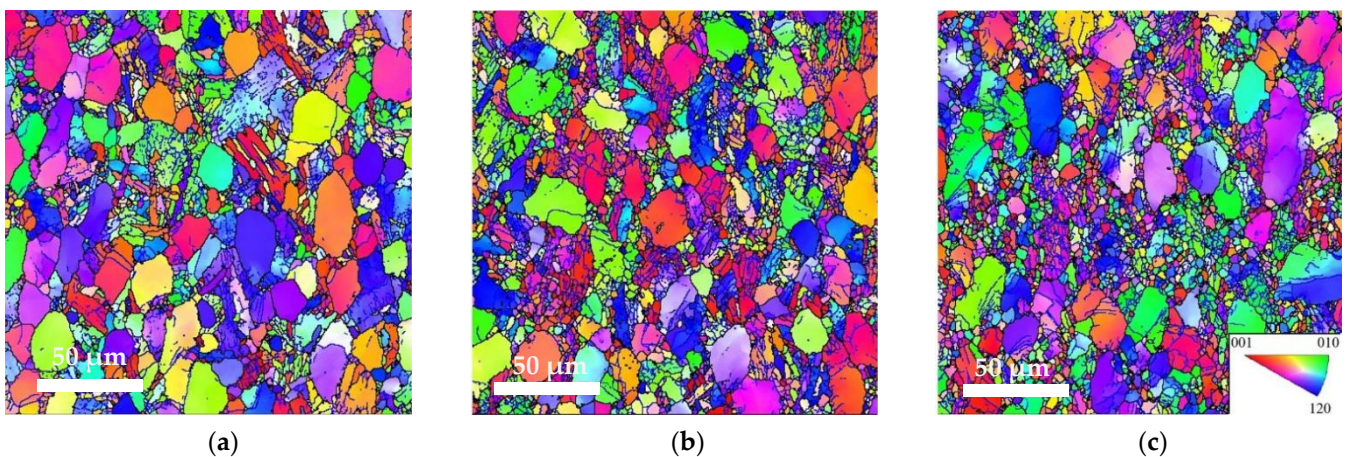


Figure 5. IPFs of specimens without pre-deformation at different true strains: (a) 0.3; (b) 0.5; and (c) 0.7.

The proportion of LAGBs first increased from 61.1% to 61.4% and then decreased from 61.4% to 58.3% when the strain increased from 0.3 to 0.7. The change in LAGBs was related to the change in dislocation density. Additionally, the evolution of dislocation density could be reflected by the geometric dislocation density (GND) [23,24]. Figure 6 shows the GND density maps of specimens without pre-deformation at true strains of 0.3, 0.5, and 0.7. The GND density first increased and then decreased. This indicates that the DRX was not obvious when the true strains were low [25]. However, a large number of deformation substructures accumulated during the initial deformation stage. The proportion increased

rapidly with the true strain beyond the critical strain, which accelerated the aggregation and growth of sub-grains, eradicated dislocations in the grains, and reduced the content of LAGBs. In addition, recrystallized grains promoted by the DRX were concentrated in the HAGBs, and only a few grains were inside the elongated grains. This suggests that high-temperature deformation can promote the migration of HAGBs and nucleation with the expansion of HAGBs. The growth in grain number depends on the grain boundary migration, which indicates that DRX is dominated by DDRX [26].

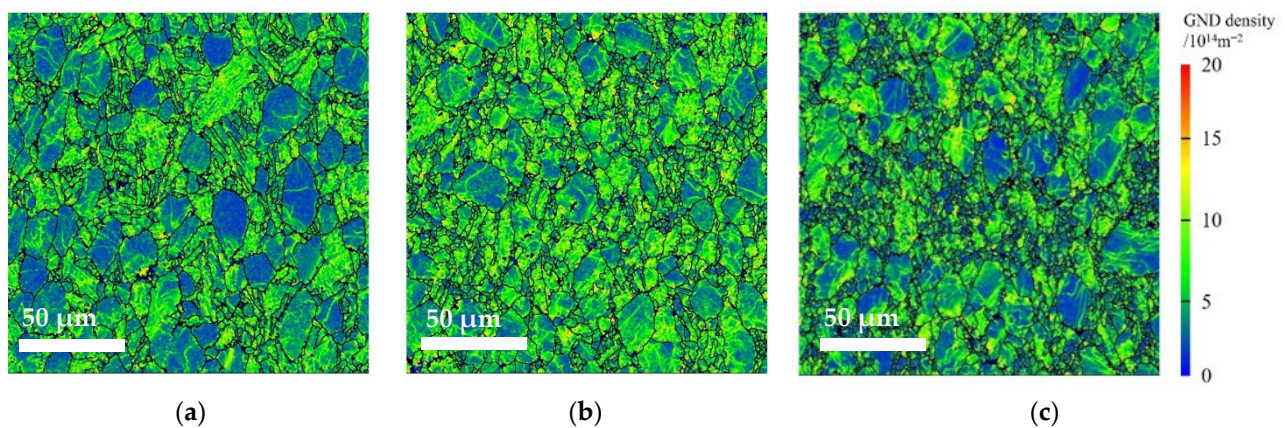


Figure 6. GND density maps of specimens without pre-deformation: (a) 0.3; (b) 0.5; and (c) 0.7.

3.2.3. Microstructure of Specimens with Pre-Strain

Figure 7 shows the IPFs of specimens with pre-strain of 0.05 at true strains of 0.3, 0.5, and 0.7. The increasing deformation promoted the DRX, leading to the formation of a large number of small grains [27,28]. Images show that the structure is mainly composed of elongated equiaxed grains and small equiaxed grains. This indicated that DRX is the main mode of microstructural evolution [29]. After the deformation, the initial grains were obviously elongated along the tensile direction, which indicated that grain boundary sliding was the main hot-deformation mechanism of Ti-6Al-4V. When the true strain rose from 0.3 to 0.5, some lamellar α grains broke and formed small equiaxed grains. When the true strain reached 0.7, the lamellar α grains were transformed into fine equiaxed grains.

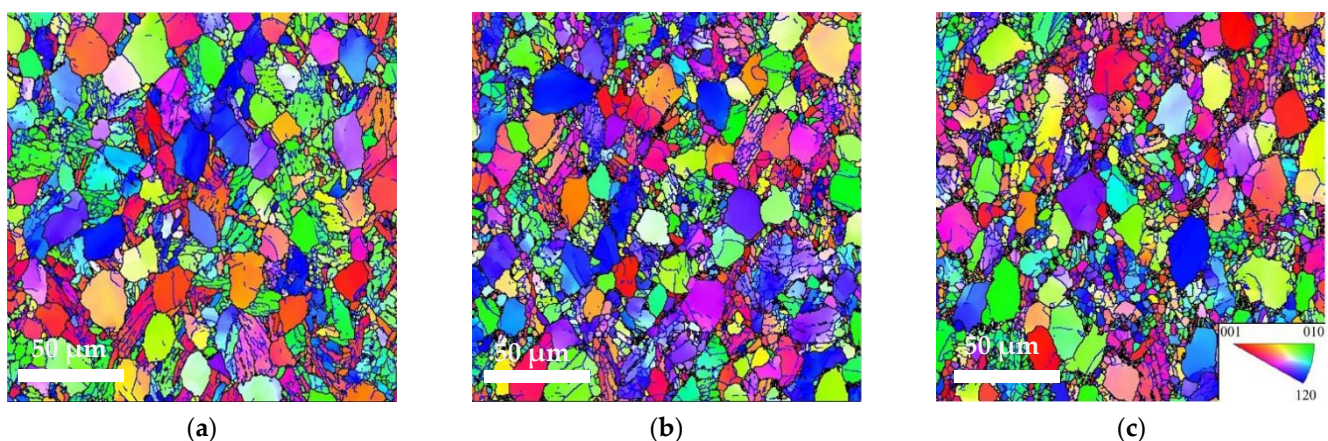


Figure 7. IPFs of specimens with pre-deformation strain of 0.05 at different true strains: (a) 0.3; (b) 0.5; and (c) 0.7.

Figure 8a shows the average grain size and dynamic recrystallization fraction of the specimens with different pre-strains. At a true strain of 0.3, the average grain sizes of the specimens with pre-strains of 0.05, 0.1 and 0.15 were 2.42 μm , 2.85 μm , and 2.79 μm , and the dynamic recrystallization fractions were 8.03%, 11%, and 12.6%, respectively. At strains

larger than 0.3, the DRX fraction increased with the decrease in pre-strain, which promoted the formation of small grains and reduced the average grain size. This caused a decrease in HAGBs, which hindered the movement of dislocations, leading to a decrease in flow stress. Figure 8b shows that the DRX fraction increased with the pre-deformation when the strain was 0.3. This indicates that the smaller pre-deformation failed to promote the DRX. However, a large number of substructures were accumulated in the material at the early stages of deformation. When the deformation continued, the substructure accelerated the annihilation and rearrangement of dislocations, leading to increased DRX [30]. Pre-deformation can promote the DRX, which accelerated the transformation of sub-grains and LAGBs into small equiaxed grains and HAGBs. With the decrease in pre-deformation, the DRX fraction increased, leading to the generation of more small-sized grains. Additionally, the increase in HAGBs, which hindered the movement of dislocations, led to the increase in strength. At the same time, the DRX fraction increased, which further intensified the softening. Compared with the specimen without pre-deformation, the pre-deformed specimens have small equiaxed grains in the largely elongated grains. It may be because the pre-deformation increased the dislocation and promoted the CDRX. In addition, more compact equiaxed grains appeared at the HAGBs, indicating that pre-deformation can effectively promote the migration of HAGBs. As the true strain promoted the DRX, during which the small grains gradually formed, the deformed substructure reduced, resulting in a gradual decrease in the flow stress. More deformed substructures were accumulated for the less pre-deformed specimens. Additionally, the increase in deformation provides the driving force for DRX.

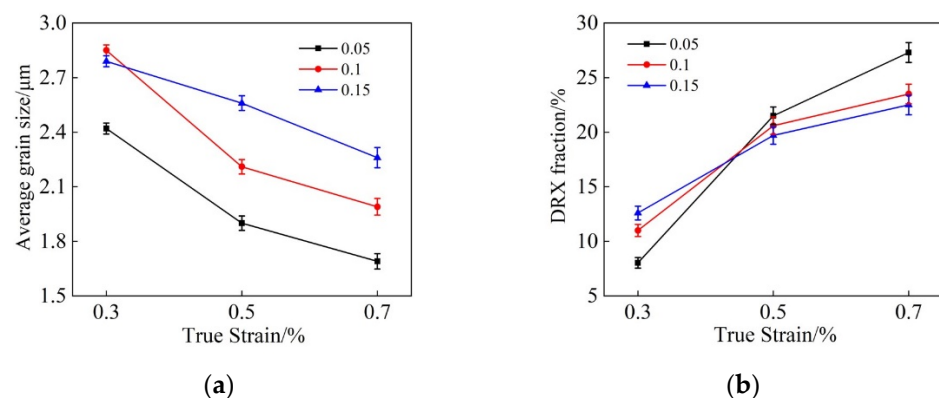


Figure 8. The (a) average grain size and (b) DRX fraction of the specimens with pre-strains.

Pre-strain can increase the deformation substructures inside the material, promote the DRX, and then reduce the dislocations in the material, so that softening occurs in the deformation process of the material and the flow stress decreases. In addition, the deformation substructure decreases with the increase in pre-strain. When the strain increases, the DRX degree of samples with smaller pre-strain is higher, and more small-sized equiaxed grains are generated. The average grain size decreases, and the proportion of HAGBs per unit area is higher, which hinders the dislocation movement and leads to the increase in flow stress.

4. Conclusions

- The deformation behavior of Ti-6Al-4V titanium alloys with different pre-deformation was studied. When the pre-strain was 0.05, the elongation of the specimen was the highest: 234.5%. When the pre-strain reached 0.15, the ultimate tensile strength was the lowest: 66.8 MPa. The hot-forming performance of Ti-6Al-4V increased first and then decreased with the increase in pre-strain;

- During the hot tensile deformation, the deformation mechanism of Ti-6Al-4V was dominated by high-angle grain boundaries sliding. Dislocation movement also played an important role in the hot deformation process, which could be considered as the adjustment process of grain boundary sliding. In the non-pre-deformed specimen, the recrystallized grains all appeared at the grain boundary, indicating that the dynamic recrystallization was dominated by discontinuous dynamic recrystallization;
- Pre-deformation provides more deformation substructures for subsequent deformation and promotes dynamic recrystallization of the material in the subsequent deformation process. Recrystallized grains appeared at the grain boundaries and inside the grains during the hot tensile process. The pre-deformation promoted both continuous dynamic recrystallization and discontinuous dynamic recrystallization, which caused major changes in mechanical properties during the hot deformation.

Author Contributions: Conceptualization, T.W., M.C., D.Z. and L.X.; methodology, N.W., D.Z. and L.X.; software, T.W. and N.W.; validation, T.W., N.W. and W.S.; formal analysis, T.W.; investigation, W.S.; resources, M.C.; data curation, T.W.; writing—original draft preparation, T.W.; writing—review and editing, T.W. and N.W.; visualization, T.W.; supervision, M.C., D.Z. and L.X.; project administration, M.C.; funding acquisition, M.C. All authors have read and agreed to the published version of the manuscript.

Funding: This research received no external funding.

Data Availability Statement: Data presented in this article are available at request from the corresponding author.

Conflicts of Interest: The authors declare no conflict of interest.

References

1. Zhao, Z.B.; Wang, Q.J.; Liu, J.R.; Yang, R. Effect of heat treatment on the crystallographic orientation evolution in a near- α titanium alloy Ti60. *Acta Mater.* **2017**, *131*, 305–314. [[CrossRef](#)]
2. Ma, L.X.; Wan, M.; Li, W.D.; Shao, J.; Bai, X.P. Constitutive modeling and processing map for hot deformation of Ti-15Mo-3Al-2.7Nb-0.2Si. *J. Alloys Compd.* **2019**, *808*, 151759. [[CrossRef](#)]
3. Cui, C.X.; Hu, B.M.; Zhao, L.C.; Liu, S.J. Titanium alloy production technology, market prospects and industry development. *Mater. Des.* **2011**, *32*, 1684–1691. [[CrossRef](#)]
4. Wang, Q.Q.; Liu, Z.Q. Plastic deformation induced nano-scale twins in Ti-6Al-4V machined surface with high speed machining. *Mater. Sci. Eng. A* **2016**, *675*, 271–279. [[CrossRef](#)]
5. Momeni, A.; Abbasi, S.M.; Sadeghpour, S. A comparative study on the hot deformation behavior of Ti-5Al-5Mo-5V-3Cr and newly developed Ti-4Al-7Mo-3V-3Cr alloys. *Vacuum* **2019**, *161*, 401–408. [[CrossRef](#)]
6. Li, W.S.; Yamasaki, S.; Mitsuhashi, M.; Hakashima, H. In situ EBSD study of deformation behavior of primary α phase in a bimodal Ti-6Al-4V alloy during uniaxial tensile tests. *Mater. Charact.* **2020**, *163*, 110282. [[CrossRef](#)]
7. Bodunrin, M.O.; Chown, L.H.; Merwe, J.W.; Alaneme, K.K. Hot working of Ti-6Al-4V with a complex initial microstructure. *Int. J. Mater. Form.* **2018**, *12*, 857–874. [[CrossRef](#)]
8. Cui, J.H.; Yang, H.; Sun, Z.C.; Li, H.W.; Li, Z.J.; Shen, W.C. Flow behavior and constitutive model using piecewise function of strain for TC11 alloy. *Rare Met. Mater. Eng.* **2012**, *41*, 397–401.
9. Liu, Z.G.; Li, P.J.; Xiong, L.T.; Liu, T.Y.; He, L.J. High-temperature deformation behavior and microstructure evolution of Ti55 titanium alloy. *Mater. Sci. Eng. A* **2016**, *680*, 259–269. [[CrossRef](#)]
10. Ma, T.F.; Zhou, X.; Du, Y.; Li, L.; Zhang, L.C.; Zhang, Y.S.; Zhang, P.X. High temperature deformation and microstructure evolution of core-shell structured titanium alloy. *J. Alloys Compd.* **2019**, *775*, 316–321. [[CrossRef](#)]
11. Wang, H.F.; Ban, C.Y.; Zhao, N.N.; Kang, Y.Y.; Qin, T.P.; Liu, S.T.; Cui, J.Z. Enhance strength and ductility of nano-grain titanium processed by two-step severe plastic deformation. *Mater. Lett.* **2020**, *266*, 127485. [[CrossRef](#)]
12. Hajizadeh, K.; Eghbali, B. Effect of two-step severe plastic deformation on the microstructure and mechanical properties of commercial purity titanium. *Met. Mater. Int.* **2014**, *20*, 343–350. [[CrossRef](#)]
13. Stolyarov, V.V.; Zeipper, L.; Mingler, B.; Zehetbauer, M. Influence of post-deformation on CP-Ti processed by equal channel angular pressing. *Mater. Sci. Eng. A* **2008**, *476*, 98–105. [[CrossRef](#)]
14. Stolyarov, V.V.; Zhu, Y.T.; Raab, G.I.; Zharikov, A.I.; Valiev, R.Z. Effect of initial microstructure on the microstructural evolution and mechanical properties of Ti during cold rolling. *Mater. Sci. Eng. A* **2004**, *385*, 309–313. [[CrossRef](#)]
15. Zhu, T.; Huang, J.Y.; Gubicza, J.; Ungar, T.; Wang, Y.M.; Ma, E.; Valiev, R.Z. Nanostructures in Ti processed by severe plastic deformation. *J. Mater. Res.* **2003**, *18*, 1908–1917. [[CrossRef](#)]

16. Wang, S.H.; Liu, C.H.; Chen, J.H.; Li, X.L.; Zhu, D.H.; Tao, G.H. Hierarchical nanostructures strengthen Al–Mg–Si alloys processed by deformation and aging. *Mater. Sci. Eng. A* **2013**, *585*, 233–242. [[CrossRef](#)]
17. Sachtleber, M.; Raabe, D.; Weiland, H. Surface roughening and color changes of coated aluminum sheets during plastic straining. *J. Mater. Process. Technol.* **2004**, *148*, 68–76. [[CrossRef](#)]
18. Seshacharyulu, T.; Medeiros, S.C.; Frazier, W.G.; Prasad, Y.V.R.K. Hot Working of Commercial Ti–6Al–4V with an Equiaxed α – β Microstructure: Materials Modeling Considerations. *Mater. Sci. Eng. A* **2000**, *284*, 184–194. [[CrossRef](#)]
19. Zhang, W.; Liu, H.; Ding, H.; Fujii, H. Superplastic Deformation Mechanism of the Friction Stir Processed Fully Lamellar Ti–6Al–4V Alloy. *Mater. Sci. Eng. A* **2020**, *785*, 139390. [[CrossRef](#)]
20. Belyakov, A.; Sakai, T.; Miura, H.; Kaibyshev, R.; Tsuzaki, K. Continuous recrystallization in austenitic stainless steel after large strain deformation. *Acta Mater.* **2002**, *50*, 1547–1557. [[CrossRef](#)]
21. Sheppard, T.; Norley, J. Deformation Characteristics of Ti–6Al–4V. *Mater. Sci. Technol.* **1988**, *4*, 903–908. [[CrossRef](#)]
22. Park, N.-K.; Yeom, J.-T.; Na, Y.-S. Characterization of Deformation Stability in Hot Forging of Conventional Ti–6Al–4V Using Processing Maps. *J. Mater. Process. Technol.* **2002**, *130–131*, 540–545. [[CrossRef](#)]
23. Kumar, S.; Pavithra, B.; Singh, V.; Ghosal, P.; Raghu, T. Tensile anisotropy associated microstructural and microtextural evolution in a metastable beta titanium alloy. *Mater. Sci. Eng. A* **2019**, *747*, 1–16. [[CrossRef](#)]
24. Moussa, C.; Bernacki, M.; Besnard, R.; Bozzolo, N. Statistical analysis of dislocations and dislocation boundaries from EBSD data. *Ultramicroscopy* **2017**, *179*, 63–72. [[CrossRef](#)] [[PubMed](#)]
25. Yi, Z.X.; Li, X.Q.; Pan, C. Dynamic Recrystallization Behavior and Model Study of Equiaxed Fine Grain Structure TC4. *J. Phys. Conf. Ser.* **2020**, *1676*, 012159. [[CrossRef](#)]
26. Sun, Y.G.; Zhang, C.J.; Feng, H.; Zhang, S.Z.; Han, J.C.; Zhang, W.G.; Zhao, E.; Wang, H.W. Dynamic recrystallization mechanism and improved mechanical properties of a near α high temperature titanium alloy processed by severe plastic deformation. *Mater. Charact.* **2020**, *163*, 110281. [[CrossRef](#)]
27. Weiss, Y.; Semiatin, S.L. Thermomechanical processing of alpha titanium alloys—An overview. *Mater. Sci. Eng. A* **1999**, *263*, 243–256. [[CrossRef](#)]
28. Zharebtsov, S.; Murzinova, M.; Salishchev, G.; Semiatin, S.L. Spheroidization of the lamellar microstructure in Ti–6Al–4V alloy during warm deformation and annealing. *Acta Mater.* **2011**, *59*, 4138–4150. [[CrossRef](#)]
29. Matsumoto, H.; Velay, V. Mesoscale modeling of dynamic recrystallization behavior, grain size evolution, dislocation density, processing map characteristic, and room temperature strength of Ti–6Al–4V alloy forged in the (α + β) region. *J. Alloys Compd.* **2017**, *708*, 404–413. [[CrossRef](#)]
30. Zhao, J.; Wang, K.H.; Huang, K.; Liu, G. Recrystallization behavior during hot tensile deformation of TA15 titanium alloy sheet with substantial prior deformed substructures. *Mater. Charact.* **2019**, *151*, 429–435. [[CrossRef](#)]